

# Structure and mechanical properties of nanostructured Al–Mg alloys processed by severe plastic deformation

Manping P. Liu · Hans J. Roven · Maxim Yu. Murashkin ·  
Ruslan Z. Valiev · Ascar Kilmametov ·  
Zhen Zhang · Yingda Yu

Received: 12 November 2012 / Accepted: 30 December 2012 / Published online: 17 January 2013  
© Springer Science+Business Media New York 2013

**Abstract** Structural features, microhardness, and mechanical properties of three binary Al–Mg alloys and a commercial AA5182 alloy subjected to high pressure torsion at room temperature were comparatively investigated using transmission electron microscopy, high-resolution transmission electron microscopy, and quantitative X-ray diffraction measurements. Average grain sizes measured by dark-field images are in the range 71–265 nm while the sizes of coherent domains decreased tremendously from 86 to 46 nm as the Mg content increased from 0.5 to 4.1 wt%. The average dislocation density in the deformed alloys is in the range  $0.37 \times 10^{14}$ – $4.97 \times 10^{14} \text{ m}^{-2}$ . Both the microhardness and tensile strength of all the deformed alloys increased dramatically as compared to the undeformed counterparts. The yield strength with values ranging from 390 to 690 MPa in the deformed alloys is typically five to seven times higher than that of the same undeformed alloys. Calculations based on the Hall–Petch and Taylor equations suggest that the strengthening mechanisms contributing to the very high strength may depend not only on the conventional mechanisms of grain size

strengthening and dislocation strengthening, but also on the additional mechanisms related to the contributions from stacking faults and nanotwins, and nonequilibrium GBs observed in the deformed alloys.

## Introduction

Over the last two decades, much progress has been made in nanostructured materials processed by severe plastic deformation (SPD) for developing nanostructures in metals and alloys with unusual properties that are very attractive for various structural and functional applications [1–7]. Significantly, the strength levels in SPD materials such as the 7075 aluminum alloy processed by high pressure torsion (HPT) have recently been entered into the ultra-high strength regime [6–10]. It is well known that Al–Mg alloys are an important class of non-heat treatable alloys (the 5xxx series) [11, 12]. They are by far the most commonly used for cryogenic tanks, aluminum siding, gutters, lighting products, memory-disk substrates, and marine engine components. Also, they are now being used for automotive applications which include inner body panels and a large number of non-structural parts due to their good recyclability, low weight, and low cost as compared to 2xxx and 7xxx aluminum alloys. Aluminum–magnesium alloys with higher Mg contents are highly desirable because of their higher tensile and fatigue strength and better weldability. Recent works have shown that Mg addition in SPD aluminum alloys enhances their properties such as the work hardening rate, thermal stability, dislocation generation, grain refinement, and thus the strength and ductility [13–17]. In addition, Al–Mg alloys are often used for studying the well-known serrated yielding or Portevin–Le Châtelier (PLC) effect and the associated plastic instabilities evident

---

M. P. Liu (✉) · Z. Zhang  
School of Materials Science and Engineering, Jiangsu Province  
Key Laboratory of High-end Structural Materials, Jiangsu  
University, 301 Xuefu Road, Zhenjiang 212013, China  
e-mail: manping-liu@263.net

H. J. Roven (✉) · Y. Yu  
Department of Materials Science and Engineering,  
Norwegian University of Science and Technology (NTNU),  
Alfred Getz vei 2b, 7491 Trondheim, Norway  
e-mail: hans.roven@material.ntnu.no

M. Yu. Murashkin · R. Z. Valiev · A. Kilmametov  
Institute of Physics of Advanced Materials, Ufa State Aviation  
Technical University, 12 K. Marx Street, Ufa 450000, Russia

during tensile flow [18]. Therefore, the binary SPD Al–Mg alloys have attracted substantial interest, both for fundamental research and technological development.

Although outstanding progress has been made in this area in recent years, there still remains an unsatisfactory fit between theory-based structure–property relationships in SPD metals [6]. It is well known that the composition has significant effects on microstructures and strengthening mechanisms subjected to SPD [2, 15, 16]. However, it is still not very obvious how mechanical properties and the microstructure features such as grain size, dislocation structures, and grain boundaries (GBs) are related to the Mg contents in nanograined Al–Mg alloys [15, 16]. For example, the veracity of Hall–Petch relationships as the grain size reduces below 100 nm is problematic [6]. This suggests strongly that the strengthening mechanisms involved in the SPD alloys may not only be related to the conventional mechanisms such as solid solution strengthening, grain size strengthening, and dislocation strengthening, but also connect with the additionally new mechanisms such as the contributions from stacking faults (SFs) and nanotwins, nonequilibrium GBs, and solute atom clusters (or solute segregations) [1, 6, 7].

In the present work, three binary Al–Mg alloys and a commercial AA5182 alloy were subjected to HPT at room temperature. The HPT-processed materials were comparatively investigated using transmission electron microscopy (TEM), high-resolution TEM (HRTEM), and quantitative X-ray diffraction (XRD) measurements. Hardness, strength, grain size distributions, dislocation densities, and densities of planar defects including SFs and nanotwins were quantified. The role of Mg on these features and the strengthening mechanisms associated with the typical nanostructures and faults were interpreted.

## Experimental

Three binary Al–Mg alloys (with 0.5, 1.0, and 2.5 wt% Mg) and a commercial AA5182 alloy (Al–4.1 Mg–0.35Mn–0.13Si–0.32Fe, by wt%) were received as rods with diameters of 20 mm in the as-cast and homogenized condition. The samples cut from the rods with diameters of 20 mm and thicknesses of 2 mm were subjected to HPT to ten turns with a rotation speed of 1 rpm under a pressure of 6 GPa at room temperature. The deformed HPT samples had dimensions of  $\sim 20$  mm in diameter and  $\sim 0.6$  mm in thickness and the calculated equivalent strain at the outer edge of the HPT samples is about 604 [2]. All the investigations of the structures and mechanical properties of the deformed HPT alloys were performed just in the regions of the samples located at half-radius from the center, i.e., at a distance of 5 mm from the sample center (Fig. 1). The

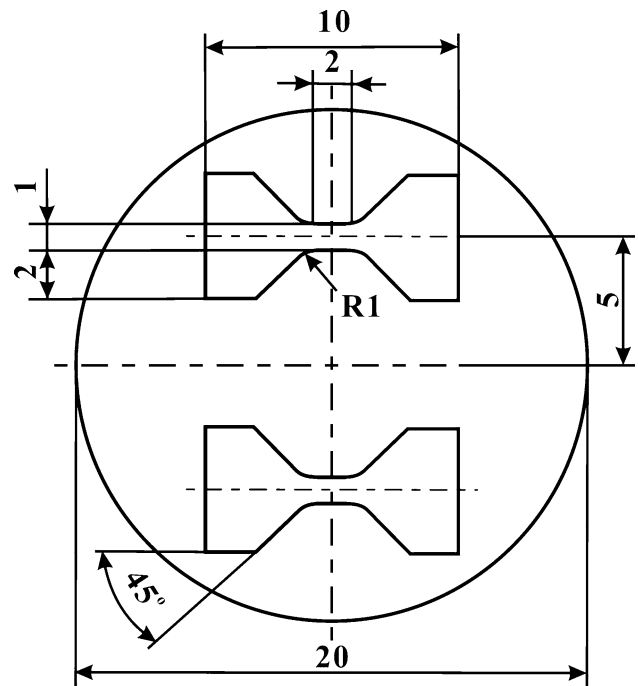


**Fig. 1** Schematic drawing of the HPT sample and the location of samples extraction for tensile tests (dimensions in millimeters)

structural characterization was performed by quantitative XRD, conventional TEM, and HRTEM. Quantitative XRD measurements were performed with a Pan Analytical X<sup>PERT</sup> diffractometer using Cu K $\alpha$  radiation at 50 kV and 40 mA. The conventional TEM was applied in both bright fields (BF) and dark fields (DF). The grain size ( $d$ ) distribution was determined from DF images with at least 100 grains. Vickers microhardness (Hv) was measured using a Micromet-5101 microindentation tester with a load of 250 mN for 15 s. Each hardness value is averaged over at least 5 measurements. Tensile tests were precisely performed using a laser extensometer at room temperature with a strain rate of  $10^{-4}$  s<sup>-1</sup> on a computer-controlled testing machine operating with a constant displacement of the specimen grips. The gauge of the tensile test samples was 2 mm in length, 1 mm in width, and 0.4 mm in thickness (Fig. 1). The yield strength (YS) ( $\sigma_{0.2}$ ), ultimate tensile strength (UTS) ( $\sigma_{UTS}$ ), and elongation ( $\delta$ ) were determined from the tests not less than three samples. The standard deviation of the tensile tests did not exceed 5 %.

## Results

### Structural features

The general microstructures in the HPT Al–Mg alloys are shown in Fig. 2. As an example, both the BF and DF

images taken from the HPT Al–0.5 Mg alloy are presented in Fig. 2a, b. For comparison, the BF image of the HPT Al–2.5 Mg alloy is simultaneously shown in Fig. 2c. These TEM micrographs demonstrate that the HPT processing of the alloys resulted in complete refinement of the initial coarse-grained structures. The histograms of grain size distribution in the HPT Al–Mg alloys obtained from DF images are shown in Fig. 3. The average grain sizes of the HPT-processed Al–0.5 Mg, Al–2.5 Mg, and AA5182 are about 265 (Fig. 3a), 86 (Fig. 3b), and 71 nm (Fig. 3c), respectively. For the HPT Al–0.5 Mg alloy, the grain size varies from 50 to 580 nm (Fig. 3a). By comparison, the microstructure in the AA5182 alloy exhibits a grain size ranging 10–180 nm (Fig. 3c). These results indicate that the content of Mg strongly influences the grain size of the investigated alloys. The average size decreased considerably from about 265 nm to 71 nm as the Mg content increased from 0.5 to 4.1 wt%. In addition, the size distributions in all the four alloys are not uniform and grains with different size coexist. The microstructures are

characterized by a log-normal size distribution and the grain size distributions may become more uniform as the Mg content increased.

The quantitative XRD measurements are shown in Table 1. The lattice parameters ( $a$ ) in both the deformed and undeformed disks increased considerably with increasing Mg contents. All lattice parameters of HPT samples are smaller than that of their undeformed counterparts due to strain effects and these changes increased with the Mg contents. For example, the lattice parameters of the deformed Al–0.5 Mg and AA5182 are about 4.0515 and 4.0683 Å, respectively (Table 1). These values are about 0.05 and 0.11 %, respectively, smaller than the lattice parameters of the undeformed counterparts.

The size of coherent domains,  $D_{\text{XRD}}$ , decreased significantly from  $86 \pm 3$  to  $46 \pm 3$  nm as the Mg content increased from 0.5 to 4.1 wt% (Table 1). It should be noted that the grain sizes ( $d$ ) in the HPT alloys measured by the DF images are often larger than the sizes ( $D_{\text{XRD}}$ ) obtained by the XRD. This difference arises because the XRD

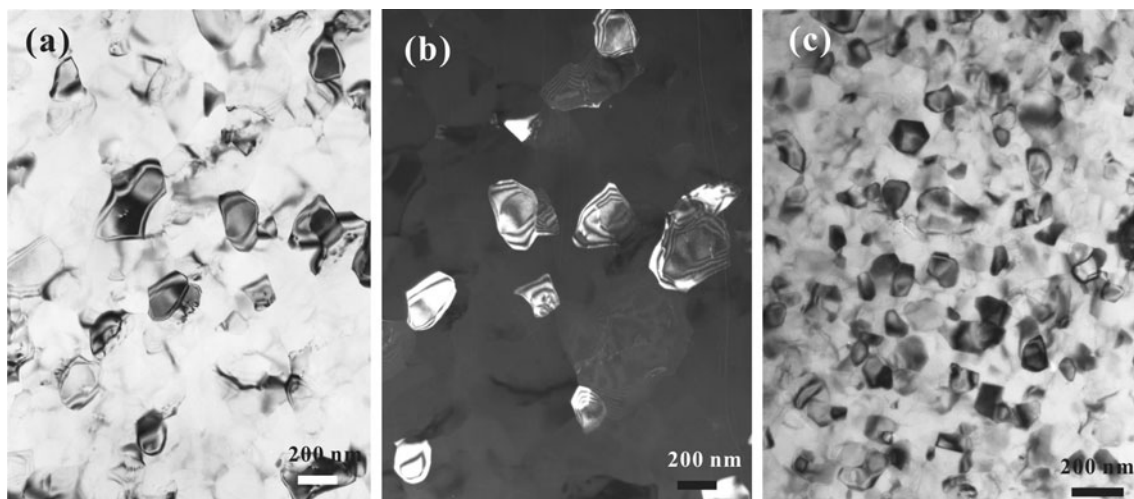


**Fig. 2** TEM micrographs of the HPT Al–Mg alloys: **a** Al–0.5 Mg alloy (BF image). **b** Al–0.5 Mg alloy (DF image). **c** Al–2.5 Mg alloy (BF image)

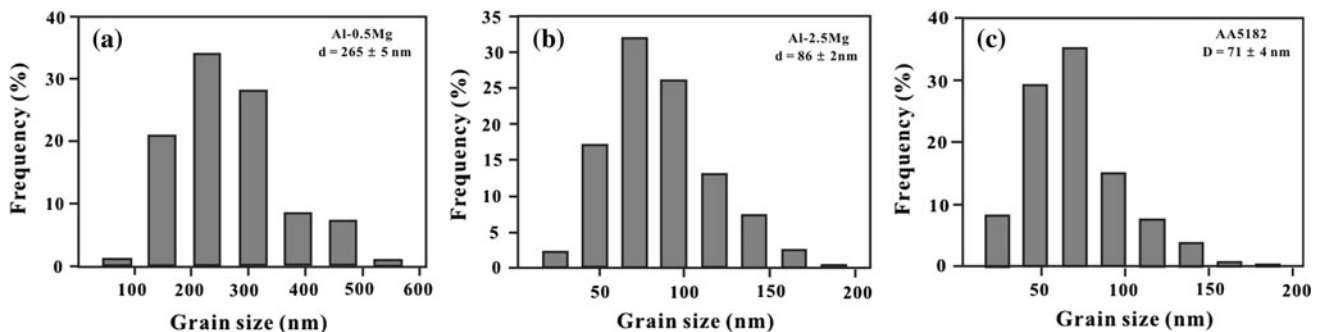


**Fig. 3** Histograms of grain size distribution in the HPT Al–Mg alloys: **a** Al–0.5 Mg alloy. **b** Al–2.5 Mg alloy. **c** AA5182 alloy

**Table 1** Microstructural characteristics of the alloys determined by the quantitative XRD method

Alloy	State	$a$ (Å)	$D_{\text{XRD}}$ (nm)	$\langle \varepsilon^2 \rangle^{1/2}$ (%)	$\rho$ (m <sup>-2</sup> )
Al-0.5 Mg	Before HPT	4.0537 ± 0.0001	–	–	–
	After HPT	4.0515 ± 0.0001	86 ± 3	0.026 ± 0.007	0.37 × 10 <sup>14</sup>
Al-1.0 Mg	Before HPT	4.0552 ± 0.0001	–	–	–
	After HPT	4.0536 ± 0.0001	75 ± 4	0.048 ± 0.011	0.77 × 10 <sup>14</sup>
Al-2.5 Mg	Before HPT	4.0635 ± 0.0001	–	–	–
	After HPT	4.0614 ± 0.0001	60 ± 4	0.120 ± 0.010	2.41 × 10 <sup>14</sup>
AA5182	Before HPT	4.0727 ± 0.0002	–	–	–
	After HPT	4.0683 ± 0.0001	46 ± 3	0.190 ± 0.010	4.97 × 10 <sup>14</sup>

process determines the size of the coherent diffraction domains and this includes both the subgrains and the dislocation cells [19–21].

The microstrain,  $\langle \varepsilon^2 \rangle^{1/2}$ , increased significantly from  $0.026 \pm 0.007$  to  $0.190 \pm 0.010$  % as the Mg content increased from 0.5 to 4.1 wt% (Table 1). Please note that, for the materials subjected to severe plastic deformation, the dislocation density is proportional to microstrain and inversely proportional to grain size [19]. Thus, the increase in microstrain indicates that the dislocation density increases with the Mg content. Using the experimentally obtained values (Table 1) of  $D_{\text{XRD}}$ ,  $\langle \varepsilon^2 \rangle^{1/2}$  and  $a$ , the dislocation density in the HPTed alloys was calculated by the formula employed in [21, 22]:

$$\rho = 2\sqrt{3} \frac{\langle \varepsilon^2 \rangle^{1/2}}{D_{\text{XRD}} b} \quad (1)$$

where  $b = a \sqrt{2}/2$  is the magnitude of the Burgers vector in the alloys.

As shown in Table 1, the calculated dislocation density increases from a minimum  $0.37 \times 10^{14} \text{ m}^{-2}$  in the deformed Al-0.5 Mg alloy to a maximum  $4.97 \times 10^{14} \text{ m}^{-2}$  in the HPTed AA5182 alloy. The dislocation densities of both the HPT Al-2.5 Mg alloy ( $2.41 \times 10^{14} \text{ m}^{-2}$ ) and AA5182 alloy are almost one order of magnitude larger than that of the deformed Al-0.5 Mg alloy, and the dislocation density of the HPT Al-1.0 Mg alloy ( $0.77 \times 10^{14} \text{ m}^{-2}$ ) is more than twice as large as that of the HPT Al-1.0 Mg alloy. All the above measurements indicate that the grain sizes, lattice parameters, microstrains, and dislocation densities of the HPT alloys are strongly influenced by the content of Mg in addition to the effects of very large strain resulting from HPT.

Our previous work revealed that deformation structures are not uniform in such HPT Al-Mg alloys [15, 16]. Different deformation structures such as dislocation-free grains, nonequilibrium grain boundaries (GBs), dislocation cell and subgrain structures, low-angle grain boundaries (LAGBs), stacking faults (SFs), and nanotwins may coexist in the alloys. Figure 4 shows a typical HRTEM image

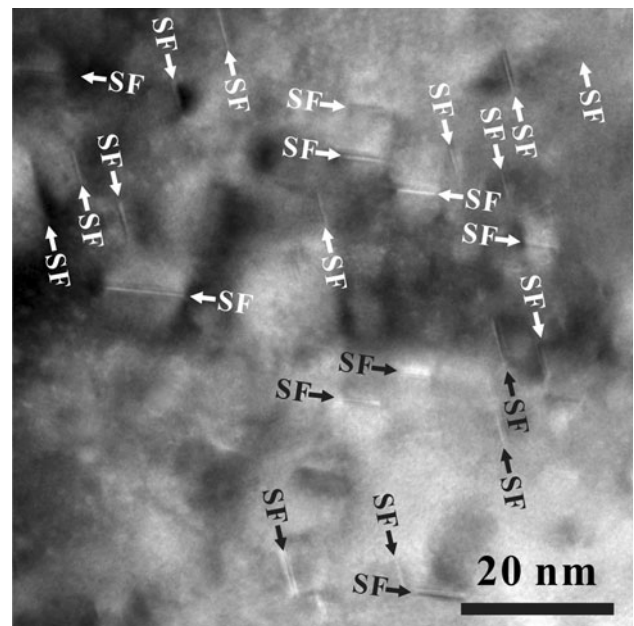


**Fig. 4** HRTEM [110] image of the HPT Al-0.5 Mg alloy, showing a high density of SFs (arrows) and nanotwins within a 200 nm grain

of such SFs and nanotwins taken from the deformed Al-0.5 Mg alloy. A high density of SFs can be seen inside a 200 nm grain. The SF widths are in the range of 5–15 nm and the local SF density is about  $10^{15} \text{ m}^{-2}$ . The SFs and microtwins seemed to be preferably located in the vicinity of GBs and sub-boundaries.

#### Mechanical properties

Table 2 presents the mechanical properties in the Al-Mg samples before and after HPT. The errors show the range of hardness values (Hv, MPa) obtained for several measurements on each sample. As shown in Table 1, the hardness increased noticeably after HPT for all samples, i.e., twice to three times higher than that of the undeformed counterparts. For example, the hardness values of the HPT-processed Al-0.5 Mg, Al-1.0 Mg, Al-2.5 Mg, and AA5182 are 1038,

1263, 1650, and 1867 MPa, respectively. These values are about 3.0, 3.1, 3.2, and 2.8 times higher than that of the undeformed counterparts (347, 406, 518, and 656 MPa). At the same time, the hardness in the HPT-processed samples increased from 1038 to 1867 MPa when the Mg content increased from 0.5 to 4.1 wt%. The hardness in HPT-AA5182 is almost two times higher than that in HPTed Al–0.5 Mg.

The results of tensile tests of the samples in the alloys both after and before HPT are presented in Fig. 5 and Table 2. Figure 5 shows typical examples of the engineering stress–strain curves of the deformed and undeformed samples and all the mechanical data are listed in Table 2. The strength and the microhardness values exhibit essentially the same tendency. Both the ultimate tensile strength and yield strength increased dramatically after HPT for all samples. The yield strength is almost five to seven times higher than that of the undeformed counterparts and the ultimate tensile strength is approximately three to five times higher than that obtained in the same undeformed alloys. For example, the YS values of the HPT-processed Al–0.5 Mg, Al–1.0 Mg, Al–2.5 Mg, and AA5182 are 390, 430, 505, and 690 MPa, respectively. These values are about 6.8, 5.7, 5.3, and 6.0 times higher than that of the undeformed counterparts (57, 75, 95, and 115 MPa). Furthermore, both the YS and UTS in the HPT-processed samples also increased considerably when the Mg content increased. The YS in HPT-AA5182 (690 MPa) is almost two times higher than that in HPTed Al–0.5 Mg (390 MPa) and the UTS increased from 490 MPa in Al–0.5 Mg to 800 MPa in HPT AA5182. These results also demonstrate that both the hardness and strength values of the HPT alloys are not only contributed by SPD, but also affected by the Mg contents. It should be note that the elongation ( $\delta$ ) decreased considerably after HPT for all the samples (Table 2) especially the values of the elongation in the deformed alloys have been smaller than 3 % when the Mg contents larger than 1 wt%. This issue should be solved by methods such as annealing in the future research and is beyond the scope of this paper.

### Discussion

Both the hardness measurements and tensile tests revealed that the mechanical properties of deformed Al–Mg samples are dramatically higher than that of their undeformed counterparts. At the same time, the hardness and strength in the HPT-processed samples increased significantly as the Mg content increased. The strengthening mechanisms involved in the deformed alloys may include solid solution strengthening, grain size strengthening, dislocation strengthening, etc. Contributions from different strengthening mechanisms are often taken to be additive assuming that they act independently, and the total strength of the present nanostructured Al alloys could be estimated as [1, 6, 7, 10, 15, 16]:

$$\sigma_{0.2} = \sigma_o + \sigma_{ss} + \sigma_{gs} + \sigma_{\rho} + \sigma_N \tag{2}$$

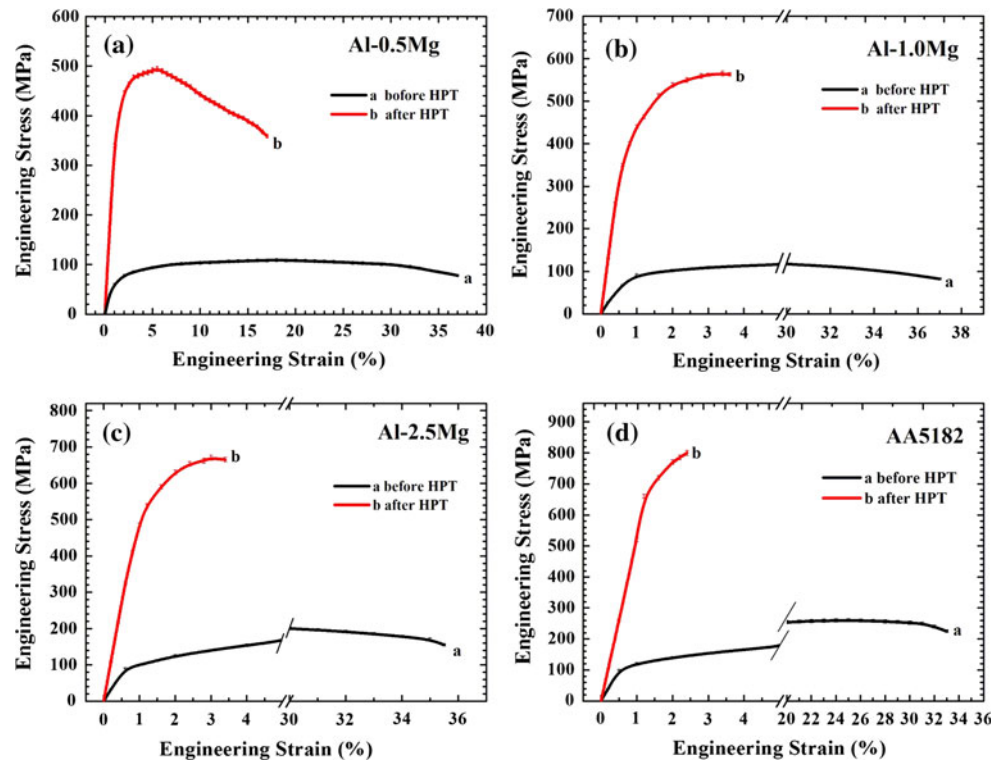
where  $\sigma_{0.2}$  is the total yield strength ( $YS_{calc}$ ),  $\sigma_o$  is the Peierls or friction stress,  $\sigma_{ss}$  is solid solution strengthening,  $\sigma_{gs}$  is grain size strengthening,  $\sigma_{\rho}$  is dislocation strengthening, and  $\sigma_N$  is the additionally new strengthening mechanisms related to the contributions from SFs and nanotwins, nonequilibrium GBs, solute atom clusters (or solute segregations), etc. The values of friction stress for all the HPT Al–Mg alloys are taken as that of pure Al (about 20 MPa) considering that other strengthening mechanisms were found to increase the friction stress in the Al alloys [1, 23].

The lattice parameter is a measure of the solid solution strengthening [24]. For the undeformed Al–Mg samples, the lattice parameter increased about 0.47 % (from 4.0537 to 4.0727 Å, Table 1) and the YS value increased about 58 MPa (from 57 to 115 MPa, Table 2, Fig. 5) as the Mg content increased from 0.5 to 4.1 wt%. However, the YS values increased dramatically after HPT for all samples though the lattice parameters of HPT samples are slightly smaller than that of their undeformed counterpart. For example, the YS value increased about 575 MPa (from 115 to 690 MPa, Table 2, Fig. 5) while the lattice parameter decreased only about 0.11 % (from 4.0727 to 4.0683 Å, Table 1) after HPT in the AA5182 sample. Therefore, solid

**Table 2** Mechanical properties of the alloys

Alloy	State	Hv (MPa)	$\sigma_{0.2}$ (MPa)	$\sigma_{UTS}$ (MPa)	$\delta$ (%)
Al–0.5 Mg	Before HPT	347 ± 12	57	105	38
	After HPT	1038 ± 10	390	490	16
Al–1.0 Mg	Before HPT	406 ± 22	75	125	37
	After HPT	1263 ± 18	430	560	2.6
Al–2.5 Mg	Before HPT	518 ± 28	95	205	35
	After HPT	1650 ± 52	505	670	2.0
AA5182	Before HPT	656 ± 27	115	255	32
	After HPT	1867 ± 48	690	800	1.0

**Fig. 5** Engineering stress–strain curves of the Al–Mg alloys before and after HPT: **a** Al–0.5 Mg alloy. **b** Al–1.0 Mg alloy. **c** Al–2.5 Mg alloy. **d** AA5182 alloy



solution strengthening may not be the main contributor to the high mechanical properties in the HPT Al–Mg alloys.

The grain size strengthening is generally described by a Hall–Petch equation [24]. As shown in Fig. 3 and Table 1, the grain size decreased tremendously with Mg contents in the HPT samples. The smaller grain size indicates that more grain or sub-grain boundaries are contributing to strengthening. The contribution of the grain size strengthening  $\sigma_{gs}$  is described by the equation based on the Hall–Petch equation [1, 24]:

$$\sigma_{gs} = Kd^{-1/2} \quad (3)$$

where  $K$  is a positive constant of yielding and  $d$  is the grain size. It was reported that  $K$  is about  $0.040 \text{ MPa m}^{1/2}$  for high-purity Al, while for less-pure Al or for Al–(2–3) Mg higher  $K$ -slopes of about  $0.07$ – $0.17 \text{ MPa m}^{1/2}$  have been proposed [23, 25]. Such an increase of  $K$ -slope was related to the presence of other strengthening mechanisms contributing to the total strength of the alloy since the Hall–Petch relation was plotted directly using the experimentally measured yield strength values [1]. Indeed, estimation of the  $K$ -slope for the original mechanism of grain boundary dislocation pile-up (by subtracting all other present strengthening contributions from the total yield strength) led to  $K = 0.06$ – $0.09 \text{ MPa m}^{1/2}$  coinciding with that value estimated in pure nanocrystalline Al [1, 26]. Therefore, the values of  $K$  in all the present HPT Al–Mg alloys are taken as  $0.040 \text{ MPa m}^{1/2}$  as that of high-purity Al [25].

According to the Eq. 3 and the values of grain size in Fig. 3, the calculated values of the grain size strengthening are about 78, 136, and 150 MPa for deformed Al–0.5 Mg, Al–2.5 Mg, and AA5182, respectively. If use the size of coherent domains (Table 1),  $D_{\text{XRD}}$ , substitute the  $d$  in Eq. 3, the calculated values of the grain size strengthening are about 136, 146, 163, and 187 MPa for deformed Al–0.5 Mg, Al–1.0 Mg, Al–2.5 Mg, and AA5182, respectively (Table 3).

Both the quantitative XRD measurements (Table 1) and the tensile tests (Table 2, Fig. 5) suggest that dislocation strengthening may contribute significantly to the strength enhancement. The excess dislocations within grains and near grain or sub-grain boundaries make dislocation glide more difficult [24]. As shown in Table 1, the dislocation density (microstrain) increased significantly with increasing Mg contents, which is consistent with the significant increase of hardness and strength in the HPT samples (Table 2, Fig. 5). The increase in the Mg content leads to an increase of Mg solute concentration and more trapped dislocations both in the grain interior and at grain boundaries [27, 28]. The contribution of the dislocation strengthening  $\sigma_{\rho}$  is usually calculated by the Taylor equation [23]:

$$\sigma_{\rho} = \alpha M G b (\rho)^{1/2} \quad (4)$$

where  $\alpha$  is a constant ( $\alpha = 0.33$  is taken),  $G$  is the shear modulus ( $G = 26 \text{ GPa}$  is taken for the Al alloys),  $b$  is the

**Table 3** Contribution of strengthening mechanisms to the strength of the HPT Al–Mg alloys

Alloy	YS <sub>exp</sub> (MPa)	σ <sub>gs</sub> (MPa)	σ <sub>ρ</sub> (MPa)	σ <sub>o</sub> + σ <sub>gs</sub> + σ <sub>ρ</sub> (MPa)	σ <sub>N</sub> (MPa)
Al–0.5 Mg	390	136	45	201	189
Al–1.0 Mg	430	146	65	231	199
Al–2.5 Mg	505	163	114	297	208
AA5182	690	187	164	371	319

length of the Burgers vector of dislocations ( $b = 0.286$  nm), and  $M$  is the Taylor factor ( $M = 3$ ). According to the Eq. 4 and the values of the dislocation density in Table 1, the calculated values of the dislocation strengthening are about 45, 65, 114, and 164 MPa for deformed Al–0.5 Mg, Al–1.0 Mg, Al–2.5 Mg, and AA5182, respectively (Table 3).

As such, the total yield strength ( $YS_{calc}$ ) contributed from the dislocation strengthening and the grain size strengthening are added up using:

$$\sigma_{0.2} = \sigma_o + \sigma_{gs} + \sigma_{\rho} \tag{5}$$

The calculated  $YS_{calc}$  values from Eq. 5 are 201, 231, 297, and 371 MPa for deformed Al–0.5 Mg, Al–1.0 Mg, Al–2.5 Mg, and AA5182, respectively. These values are much smaller than the experimental  $YS_{exp}$  values 390, 430, 505, and 690 MPa for deformed Al–0.5 Mg, Al–1.0 Mg, Al–2.5 Mg, and AA5182, respectively (Table 2 and Table 3).

The above calculations indicate that the conventional strengthening mechanisms from the dislocation strengthening and the grain size strengthening only provide about 50 % of the total strength (Table 3). This means that additionally new strengthening mechanisms should be accounted for another about 50 % for the total strength in the present HPT alloys (see  $\sigma_N$  in Table 3). These new strengthening mechanisms may be related to the contributions from SFs and nanotwins, nonequilibrium GBs, and solute atom clusters (or solute segregation).

As shown in Fig. 4, a high density of planar defects including SFs and nanotwins was frequently detected within both nanocrystalline grains and ultrafine grains in all the HPT Al–Mg samples. These planar defects could have a considerable effect on the strengthening. Similar to the role of grain boundaries, the new interfaces introduced by these planar defects can act as strong barriers to block dislocation movements [1, 10], which further enhance the grain refinement strengthening and dislocation strengthening.

At the same time, non-equilibrium GBs were often present in our SPD Al–Mg alloys [15, 16]. Non-equilibrium GBs are those possessing excess energy, long-range stresses, and enhanced free volume; the formation of which typically results from interaction of lattice dislocations and grain boundaries [1]. The dislocations trapped near the non-equilibrium GBs are referred to as “extrinsic dislocations” because there are more dislocations than required to geometrically accommodate the misorientation across the

boundaries [29, 30]. The non-equilibrium GBs introduced into material during SPD processing and increased participation of extrinsic dislocations in plastic deformation might also affect the strengthening [1]. The contribution of the strengthening from non-equilibrium GBs is recently provided by Valiev et al. as [31]:

$$\sigma_{\rho_{NGB}} = \alpha M G b (\rho_{NGB})^{1/2} \tag{6}$$

where  $\rho_{NGB}$  is the density of extrinsic GB dislocations. Our previous HRTEM observations revealed that local dislocation densities in non-equilibrium GBs might be in the range of  $10^{16}$ – $10^{17}$  m<sup>-2</sup> [15, 32]. Thus the contribution of this mechanism to the YS could be larger than 700 MPa according to Eq. 6. This estimation clearly indicates that non-equilibrium GBs play an important role in the strength of the SPD nanostructured Al alloys though it over predicts the strength increase.

In addition, recent investigations using 3D-atom probe technique directly testify to the formation of solute atom clusters (or solute segregations) of impurities and alloying elements in the Al alloys processed by SPD [1, 6, 7]. In the SPD-processed Al alloys, the clusters are located at GBs and triple junctions and have higher local concentrations of solute atoms [1]. These segregations form clusters ~3–5 nm in size and influence the formation and motion of dislocations which accordingly leads to additional strengthening of the nanostructured Al alloys [1]. It was recently reported that the contribution of this mechanism to strengthening could be large up to 40–50 % of the yield strength of the SPD nanostructured Al alloys [33].

### Summary

The structural features, microhardness, and tensile strength of the HPT alloys are not only contributed by SPD, but also affected by the content of Mg. Average grain sizes measured by dark-field images are in the range 71–265 nm while the sizes of coherent domains decreased tremendously from 86 to 46 nm as the Mg content increased from 0.5 to 4.1 wt%. The average dislocation density in the deformed alloys is in the range  $0.37 \times 10^{14}$ – $4.97 \times 10^{14}$  m<sup>-2</sup> as the Mg content increased. Both the microhardness and tensile strength of all the deformed alloys increased dramatically as compared to the undeformed counterparts.

The yield strength with values ranging from 390 to 690 MPa (the maximum YS value obtained in the HPTed AA5182 alloy) in the deformed alloys is typically five to seven times higher than that of the same undeformed alloys. However, the elongation ( $\delta$ ) decreased considerably after HPT for all the samples, especially the values of the elongation in the deformed alloys have been smaller than 3 % when the Mg contents is larger than 1 wt%. Calculations based on the Hall–Petch and Taylor equations suggest that the strengthening mechanisms contributing to the very high strength may depend not only on the conventional mechanisms of grain size strengthening and dislocation strengthening, but also on the additional mechanisms related to the contributions from stacking faults and nanotwins, and nonequilibrium GBs observed in the deformed alloys.

**Acknowledgements** This work was supported by the National Natural Science Foundation of China (grant 50971087), the Basic Research Program (Natural Science Foundation) of Jiangsu Province (grant BK2012715), the Senior Talent Research Foundation of Jiangsu University (grant 11JDG070), and the Research Council of Norway under the NEW Light Metals of the Strategic Area Materials (grant 10371800). The authors also want to acknowledge the assistance of Dr. Lilya Kurmanaeva (Forschung Center of Karlsruhe, Germany) for doing the tensile testing.

## References

- Sabirov I, Murashkin MYu, Valiev RZ (2013) *Mater Sci Eng, A* 560:1
- Valiev RZ, Islamgaliev RK, Alexandrov IV (2000) *Prog Mater Sci* 45:103
- Liu MP, Roven HJ, Yu YD (2008) *Intern J Mater Res* 98:184
- Liu MP, Roven HJ (2007) *Appl Phys Lett* 90:083115
- Liu MP, Roven HJ, Yu YD, Werenskiold JC (2008) *Mater Sci Eng, A* 483–484:59
- Liddicoat PV, Liao XZ, Zhao YH, Zhu YT, Murashkin MY, Lavernia EJ, Valiev RZ, Ringer SP (2010) *Nat Commun* 1:63
- Hu LJ, Zhao SJ (2012) *J Mater Sci* 47:6872
- Zhu T, Li J (2010) *Prog Mater Sci* 55:710
- Suresh S, Li J (2008) *Nature* 456:716
- Lu L, Chen X, Huang X, Lu K (2009) *Science* 323:607
- Liu XY, Adams JB (1998) *Acta Mater* 46:3467
- Liu XY, Ohotnicky PP, Adams JB, Rohrer CL, Hyland RW Jr (1997) *Surf Sci* 373:357
- Zhang JW, Starink MJ, Gao N, Zhou WL (2011) *Mater Sci Eng, A* 528:2093
- Youssef KM, Scattergood RO, Murty KL, Koch CC (2006) *Scr Mater* 54:251
- Liu MP, Roven HJ, Liu XT, Murashkin M, Valiev RZ, Ungár T, Balogh L (2010) *J Mater Sci* 45:4659
- Liu MP, Roven HJ, Murashkin M, Valiev RZ (2009) *Mater Sci Eng, A* 503:122
- Zhou F, Liao XZ, Zhu YT, Dallek S, Lavernia EJ (2003) *Acta Mater* 51:2777
- Kovács Zs, Chinh NQ, Lendvai J, Horita Z, Langdon TG (2002) *Mater Sci Forum* 396–402:1073
- Ungár T (2007) *J Mater Sci* 42:1584
- Zhao YH, Horita Z, Langdon TG, Zhu YT (2008) *Mater Sci Eng, A* 474:342
- Murashkin M, Kil'mametov AR, Valiev RZ (2008) *Phys Met Metall* 106:90
- Zhilyaev AP, Langdon TG (2008) *Prog Mater Sci* 53:893
- Gubicza J, Chinh NQ, Krállics Gy, Schiller I, Ungár T (2006) *Curr Appl Phys* 6:194
- Zhao YH, Liao XZ, Jin Z, Valiev RZ, Zhu YT (2004) *Acta Mater* 52:4589
- Gutierrez-Urrutia I, Munoz-Morris MA, Morris DG (2006) *J Mater Res* 21:329
- Shanmugasundaram T, Heilmaier M, Murty BS, Subramanya Sarma V (2010) *Mater Sci Eng, A* 527:7821
- Chandler HD, Bee JV (1987) *Acta Metall* 35:2503
- Olmsted DL, Hector LG Jr, Curtin WA (2006) *J Mech Phys Solids* 54:1763
- Valiev RZ, Gertsman VY, Kaibyshev OA (1986) *Phys Status Solidi A* 97:11
- J. Y. Huang JY, Y. T. Zhu YT, H. Jiang H, T. C. Lowe TC (2001) *Acta Mater* 49:1497
- Valiev RZ, Enikeev NA, Langdon TG (2011) *Kovove Mater* 49:1
- Liu MP, Roven HJ, Ungár T, Balogh L, Murashkin M, Valiev RZ (2008) *Mater Sci Forum* 584–586:528
- Valiev RZ, Enikeev NA, MYu Murashkin, Kazykhanov VU, Sauvage X (2010) *Scr Mater* 63:949